Freezing of a Binary Alloy Saturating a Packed Bed of Spheres

W-Z. Cao* and D. Poulikakos†
University of Illinois at Chicago, Chicago, Illinois 60680

The phenomenon of solidification of a binary alloy (water and ammonium chloride) saturating a packed bed of spheres is investigated experimentally. The system is cooled through its top surface. The effect of heating the bottom surface of the system simultaneously with cooling its top surface is also examined. Three distinct regions were observed in the bed of spheres during the freezing process. A solid region adjacent to the cold top surface, a mixed phase region (commonly termed the "mush" or "mushy zone") consisting of a mixture of solidified alloy and liquid, and a liquid region. The mixed-phase region separated the solid and liquid regions and was of significant extent. The temperature distribution in the solid and in the mixed-phase regions was practically linear. Increasing the initial concentration of the system or heating the bottom wall had the effect of retarding the rate of solidification. Interestingly, *remelting* was observed at the solid/mush and mush/liquid interfaces. A comparison of the experimental results to a simple analytical model that neglected the presence of convection had reasonable success in the solid and mushy regions and no success in the liquid region, except at early times, when convection was not dominant. In addition, the theoretical model did not predict accurately the growth of the solid/mush and mush/liquid interfaces during the time when remelting occurred. However, if rough estimates of the growth rates are desired, the analytical model may be used to provide those estimates.

Nomenclature

C = concentration of solute, wt %
C_i = initial concentration, wt %
C_p = specific heat, J/(kgK)
G = dimensionless latent heat of fusion
H = height of the cavity, mm
k = thermal conductivity, W/(mK)
L = latent heat of fusion
Q = heat transfer rate through the bottom wall
T = temperature, °C
T_{eq} = equilibrium temperature corresponding to the initial concentration of solute (liquidus line), °C
T_{eut} = eutectic temperature
T_i = initial solution temperature
T_T = top plate wall temperature
T_0 = melting temperature of pure ice (0°C)
t = time, s
R_{cp2} = ratio of the volumetrically averaged specific heat of the mush to that of the solid region
R_{cp3} = ratio of the volumetrically averaged specific heat of the liquid to that of the solid region
R_{k2} = ratio of the volumetrically averaged thermal conductivity of the mush to that of the solid region
R_{k3} = ratio of the volumetrically averaged thermal conductivity of the liquid to that of the solid region
x = space coordinate
α = thermal diffusivity
β_2, β_3 = dimensionless group, Eq. (25)
η = similarity variable, Eq. (19)
Θ_1, Θ_2, Θ_3 = dimensionless group, Eq. (25)
ρ = density
ϕ = porosity
χ = solid fraction

Subscripts

b = glass bead
ℓ = liquid phase of the water-NH_4Cl alloy
m = mixed (mushy) phase of the water-NH_4Cl alloy
$m\ell$ = mush/liquid interface
s = solid phase of the water-NH_4Cl alloy
sm = solid/mush interface
1 = solid region
2 = mixed-phase region
3 = liquid region

Received April 12, 1989; revision received July 5, 1989.

*Graduate Student, Mechanical Engineering Department.
†Associate Professor, Mechanical Engineering Department.

I. Introduction

FREEZING of mixtures and alloys saturating a solid permeable matrix has applications in the chemical industry, geology (freezing of soils and rocks), and the food industry (production and preservation of various food products). From the heat and mass transport standpoint, the freezing of a mixture saturating a porous matrix constitutes a process with several intricacies. The phase change process occurs in the pores of the solid matrix, and it is such that three distinct regions come to existence. In the first region, the pores of the matrix are occupied by the frozen solid. In the second region, often termed the mixed-phase region or the mushy zone, the pores of the solid matrix are occupied by a complex composite of solid freckles or dendrites and liquid. Here, heat transfer involves three different phases, namely, the solid constituting the matrix, the solid constituting the freckles or dendrites, and the liquid. Fluid motion is clearly possible in the mushy region. The third region is simply the part of the porous matrix saturated with the liquid that has not been solidified yet. The mixed-phase region separates the solid from the liquid regions.

Even though the present work pertains to freezing of a mixture in a bed of packed spheres, some of the relevant work on solidification of liquid mixtures in the absence of a solid matrix (such as the bed of beads mentioned above) will be reviewed first. O'Callaghan et al.[1] used a model that accounts for the mushy zone to study theoretically heat and mass transfer during solidification of a eutectic binary solution. The speed of propagation of the liquid/mush interface was taken to be identical to the speed of propagation of the solid/liquid interface. Fang et al.[2] reported an experimental and theoretical

study of the selective freezing of a dilute solution on a cold ice surface. The comparison between theory and experiment showed good agreement. Worster[3] investigated theoretically the effect of the mushy zone on the solidification of an alloy cooled from below. His model accounted for the simultaneous action of heat and mass diffusion. Also theoretical was the work of Poulikakos[4] and Poulikakos and Cao[5] on the heat and mass transfer process during the growth of a solid from a thin pipe or wire immersed in a binary alloy. The mixed-phase region proved to be of paramount importance on the resulting solid growth rate. Bennon and Incropera[6] derived a set of continuum conservation equations for binary solid-liquid phase change systems by integrating semiempirical laws and microscopic descriptions of transport behavior with principles of classical mixture theory. The same authors[7] used these conservation equations to model and solve numerically the problem of solidification of a binary alloy in a cavity cooled through one of its side walls. Hayashi and Komori[8] investigated experimentally the freezing of a salt solution in cells. The presence of a sizable mushy zone growing with time was observed. A simple, diffusion-based theoretical model predicted growth rates that compared acceptably with those of the experiments. Additional work pertinent to the study of the mushy zone that has been reported in the literature is exemplified by Refs. 9–11.

With reference to freezing within a permeable solid matrix, our literature survey indicated that to a large extent published heat transfer works focus on the freezing of pure substances. Gupta and Churchill[12] studied the heat and moisture transfer in wet sand during freezing. The water migrated to the freezing front and froze out, producing an increase in the water content of the frozen sand and a decrease in the water content of the nonfrozen sand. Frivik and Comini[13] tackled the combined problem of freezing of soil in the presence of water flow computationally and experimentally. An analytical solution based on the complex variable theory was employed by Goldstein and Reid[14] to study the phase change of a water-saturated porous bed in the presence of a seepage flow. This study showed how the fluid flow affected the growth rate and shape of the frozen layer. Sugawara et al.[15] examined the effect of maximum density of water on freezing of a water-saturated horizontal porous layer. The comparison betwen theory and experiment was rather successful. Weaver and Viskanta[16,17] studied the freezing of a liquid-saturated bed of beads filling a rectangular and a cylindrical enclosure. Their results showed that the porous matrix suppressed the bicellular flow. The convection at the liquid region had a visible effect on the shape and the motion of the solid-liquid interface.

The present paper presents the main results of an experimental investigation on the freezing of a packed bed of spheres saturated by a water-NH_4Cl mixture and cooled through its top wall. The effect of simultaneous heating through the bottom wall of the bed is also investigated. The main results of this paper illuminate the effect of initial mixture concentration on the transient solidification phenomenon and document the temperature history and composition (solid-mushy and liquid regions) of the solidifying system.

II. Apparatus and Procedure

The experimental apparatus consisted of a test section and three supporting devices. The three supporting devices were a data acquisition system, a power supply, and a bath refrigerator circulator.

The internal dimensions of the rectangular test apparatus measured 48.3 cm long by 25.4 cm tall by 12.7 cm deep. Plexiglas (low thermal conductivity), 1.27 cm thick, was used to construct the side walls of the apparatus so that these walls did not alter the vertical heat transport. The top and the bottom walls were constructed out of aluminum of thicknesses 2.54 cm and 1.27 cm, respectively. The bottom plate had 10 (T-type) thermocouples embedded 1.6 mm from the inside surface. Machined into the bottom plate was a cavity for a 3.2-mm-thick, high-density (10 W/in.^{2}) flexible rubber electric heater. Highly conductive silicon paste was used to ensure good conductivity between the heater and the aluminum plate. The heater was insulated from below with two layers of 8-mm-thick asbestos gasket material and a layer of 16-mm-thick rubber insulation. Taking into account the fact that the thermal conductivity of asbestos [0.15 (W/m°C)] and the thermal conductivity of rubber [0.02 (W/m°C)] are much smaller than the thermal conductivity of aluminum [200 (W/m°C)] and water [0.6 (W/m°C)], we estimated the heat leak from the heater to the environment, i.e., the portion of the heating power not going into the enclosure. The heat leak to the environment was always less than 5% of the total heating power. This estimate is conservative because it does not account for the fact that the enclosure was situated on top of a 50-mm-thick wooden table top. The presence of the heater allowed for heating from below (whenever desirable) simultaneously with cooling from above. This heating effect strengthened the buoyancy-driven flow in the liquid phase and helped to contrast its effect to experiments in which no heating from below existed.

The top plate was machined to allow for eight thermocouples and a counterflow heat exchanger. The counterflow heat exchanger was constructed by milling four channels into the top plate lengthwise. A 50% ethylene glycol/water solution precooled by the bath refrigerator was circulated through the heat exchanger. The direction of flow of the coolant was alternated in adjacent channels to establish isothermality (within 0.5°C) along the top plate. The channels were sealed with a 1.27-cm-thick sheet of Plexiglas that covered the entire top plate.

Placed within the cavity were two vertical plastic rods on each of which 25 thermocouples were mounted. These two thermocouple columns allowed for the determination of transient temperature distributions in the vertical direction. One thermocouple column was placed at the centerline of the cavity. The other was in the middle of the left half of the cavity.

Before the beginning of each experiment, the soda lime beads (3 mm in diameter) were carefully inserted and packed in the test section. This resulted in a porous matrix of uniform porosity $\phi = 0.38$. Next, the water-NH_4Cl solution of a constant predetermined concentration completely filled the test section. Four different concentrations were used in the course of the study: 0, 5, 10, and 15% weight. After the filling process was completed, the system was left to settle for a few hours. The experiments began with circulating the coolant (a solution of water and ethylene glycol) precooled by the refrigerator-circulator to a desired temperature (−25°C for the majority of the experiments) through the top wall heat exchanger. If heating the bottom wall was desired, the power supply connected to the bottom wall heater was turned on at the same time that the cooling of the top wall was started. Measuring the voltage across and the current through the heater allowed for the determination of the heating power. Two separate series of experiments were performed. One corresponding to an insulated bottom wall ($Q = 0$) and another to a heated bottom wall with $Q = 36$ W.

The temperature field in the cavity and the walls was monitored by thermocouple arrays and the data acquisition system described earlier. The thicknesses of the solid and the mushy zones at the centerline and at 50 mm to the right of the centerline were measured every 30 min with the help of a precision ruler attached to the front Plexiglas wall of the apparatus. The experiment was terminated at any desired time before complete freezing (disappearance of the liquid phase) of the mixture in the system. The accuracy of the temperature measurements was estimated to be within 3% and was dictated by the accuracy of the software that converted voltage measurements to temperature measurements. The measurements of the thicknesses of the solid and the mushy regions were estimated to be accurate within 5%.

III. Simple Theoretical Model

In this section a simple theoretical model is presented that will be tested against the experimental results. A schematic of the theoretical model is shown in Fig. 1. This model neglects the presence of convection in the system. In addition, it is based on the following assumptions:

1) Equilibrium conditions exist locally in the mixed-phase region, so that the temperature-concentration relation in this region is described by the equilibrium phase diagram[18] (Fig. 2).

2) The solid fraction and the amount of internal heat generation corresponding to the latent heat of fusion released in the mushy zone are functions of temperature only.

3) The properties of the mushy zone are assumed to be volume fraction weighted averages of the properties of the individual phases. This includes the solid matrix consisting of glass beads.

4) The densities of the solid and liquid phase do not differ appreciably.

5) The liquid region is of very large extent, i.e., the presence of the bottom wall is not taken into account.

6) The effect of the species diffusion on the solidification process is neglected. This assumption is justified by the fact that for water-salt mixtures the thermal diffusivity of the mixture is much larger than the species diffusivity.[2]

Based on the preceding assumptions, the governing equations for heat diffusion in the system are

Solid region $0<x<x_{sm}$:

$$(\rho C_p)_1 \frac{\partial T_1}{\partial t} = k_1 \frac{\partial^2 T_1}{\partial x^2} \tag{1}$$

Mixed-Phase region $x_{sm}<x<x_{m\ell}$:

$$(\rho C_p)_2 \frac{\partial T_2}{\partial t} = k_2 \frac{\partial^2 T_2}{\partial x^2} + \rho_1 L \phi \frac{\partial x}{\partial T_2} \frac{\partial T_2}{\partial t} \tag{2}$$

Liquid region $x>x_{m\ell}$:

$$(\rho C_p)_3 \frac{\partial T}{\partial t} = k_3 \frac{\partial^2 T_3}{\partial x^2} \tag{3}$$

The second term in the right side of Eq. (2) expresses the release of latent heat of fusion in the mushy zone.

The effective thermal conductivity and the specific heat of the aforementioned three regions are

Solid region $0<x<x_{sm}$:

$$k_1 = \phi k_s + (1-\phi)k_b \tag{4}$$

$$C_{p1} = \phi C_{ps} + (1-\phi)C_{pb} \tag{5}$$

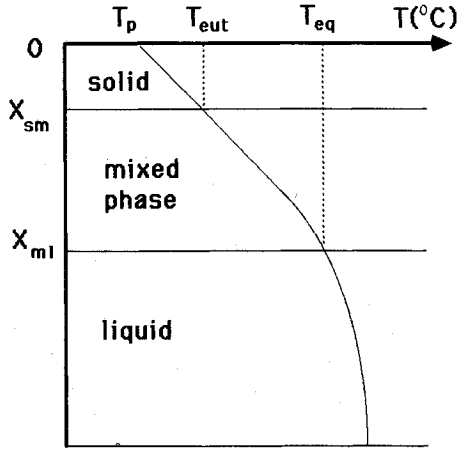

Fig. 1 Schematic of the simplified problem modeled theoretically.

Mixed-Phase region $x_{sm}<x<x_{m\ell}$:

$$k_2 = \phi k_m + (1-\phi)k_b \tag{6}$$

$$C_{p2} = \phi C_{pm} + (1-\phi)C_{pb} \tag{7}$$

where

$$k_m = \chi k_s + (1-\chi)k_\ell \tag{8}$$

$$C_{pm} = \chi C_{ps} + (1-\chi)C_{p\ell} \tag{9}$$

Liquid region $x_{m\ell}<x<\infty$:

$$k_3 = \phi k_\ell + (1-\phi)k_b \tag{10}$$

$$C_{p3} = \phi C_{p\ell} + (1-\phi)C_{pb} \tag{11}$$

Note that the use of volume-weighted effective properties in Eqs. (4–11) is common practice in the study of heat transfer in packed beds and is especially appropriate for the present study since the densities of water, ice, and soda lime are of the same order of magnitude.

The initial and boundary conditions necessary to complete the formulation of the model are

$$T_1(0,t) = T_T \tag{12}$$

$$T_1(x_{sm},t) = T_2(x_{sm},t) = T_{\text{eut}} \tag{13}$$

$$k_1\left(\frac{\partial T_1}{\partial x}\right)_{x_{sm}} - k_2\left(\frac{\partial T_2}{\partial x}\right)_{x_{sm}} = \rho\phi L(1-\chi_{sm})\frac{dx_{sm}}{dt} \tag{14}$$

$$T_3(x,0) = T_i \tag{15}$$

$$T_2(x_{m\ell},t) = T_3(x_{m\ell},t) = T_{\text{eq}} \tag{16}$$

$$k_2\left(\frac{\partial T_2}{\partial x}\right)_{x_{m\ell}} - k_3\left(\frac{\partial T_3}{\partial x}\right)_{x_{m\ell}} = \rho\phi L \chi_{m\ell}\frac{dx_{m\ell}}{dt} \tag{17}$$

Clearly, the matching conditions stated above at the solid/mush and mush/liquid interfaces stand for continuity of temperature and discontinuity of heat flux because phase change occurs at these interfaces.

The solid fraction χ is related to the concentration in the mushy zone with the help of

$$\chi = [C(T) - C_i]/C(T) \tag{18}$$

where $C(T)$ is determined from the equilibrium phase diagram for the NH_4Cl-water solution (Fig. 1). The equilibrium phase

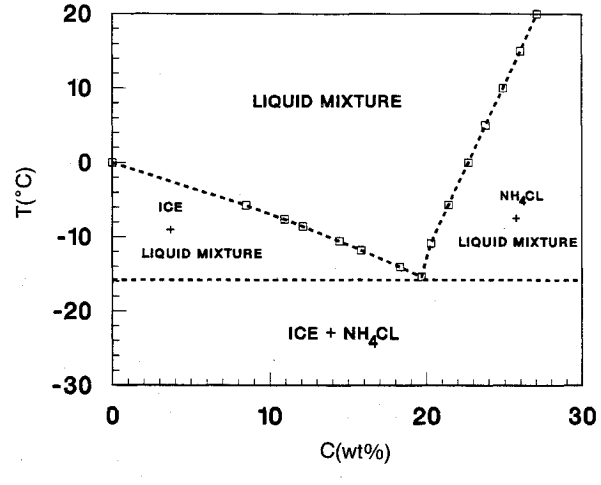

Fig. 2 Equilibrium phase diagram for a water-NH_4Cl eutectic binary alloy.

diagram is also used to obtain the value of $\partial\chi/\partial T_2$ in the right side of Eq. (2). Clearly, χ depends on temperature. For the sake of simplicity, an average value for χ and for $\partial\chi/\partial T_2$ was used in the numerical calculations. This approximation is better for higher values of C_i. It was calculated but not shown here for brevity that the dependence of χ on temperature weakens as the value of C_i increases. The average values of χ and $\partial\chi/\partial T_2$ used in the calculations were simply the arithmetic means of the values of these parameters at the solid/mush and the mush/liquid interfaces. These values as well as the values of all the parameters used in the theoretical model taken from Refs. 18-20 are reported in Table 1.

To obtain the solution of the model described, the following similarity variable is introduced:

$$\eta = \frac{x}{2\sqrt{\alpha_1 t}} \tag{19}$$

The equations and boundary conditions are next transformed with the help of the similarity variable, and the problem reduces to the solution of a system of three ordinary differential equations. The procedure is straightforward[2] and will not be repeated here for brevity. The final results read

$$T_1(\eta) = T_T + (T_{\text{eut}} - T_T)\frac{\text{erf}(\eta)}{\text{erf}(\eta_{sm})} \tag{20}$$

$$T_2(\eta) = \frac{T_{\text{eut}}\text{erf}(\sqrt{\beta_2}\eta_{m\ell}) - T_{\text{eq}}\text{erf}(\sqrt{\beta_2}\eta_{sm}) + (T_{\text{eq}} - T_{\text{eut}})\text{erf}(\sqrt{\beta_2}\eta)}{\text{erf}(\sqrt{\beta_2}\eta_{m\ell}) - \text{erf}(\sqrt{\beta_2}\eta_{sm})} \tag{21}$$

$$T_3(\eta) = T_i + (T_{\text{eq}} - T_i)\frac{\text{erf}(\sqrt{\beta_3}\eta)}{\text{erfc}(\sqrt{\beta_3}\eta_{m\ell})} \tag{22}$$

The constants $\eta_{m\ell}$ and η_{sm} are obtained from the numerical solution of the following nonlinear algebraic equations [obtained from matching conditions, Eqs. (14-17)]:

$$\frac{\Theta_1 e^{-\eta_{sm}^2}}{\text{erf}(\eta_{sm})} - \frac{\sqrt{\beta_2}R_{k2}\Theta_2 e^{-\beta_2\eta_{sm}^2}}{\text{erf}(\sqrt{\beta_2}\eta_{m\ell}) - \text{erf}(\sqrt{\beta_2}\eta_{sm})} = = \sqrt{\pi}\phi G\eta_{sm}(1-\chi_{sm}) \tag{23}$$

$$\frac{\sqrt{\beta_2}R_{k2}\Theta_2 e^{-\beta_2\eta_{m\ell}^2}}{\text{erf}(\sqrt{\beta_2}\eta_{m\ell}) - \text{erf}(\sqrt{\beta_2}\eta_{sm})} + \frac{\sqrt{\beta_3}R_{k3}\Theta_3 e^{-\beta_3\eta_{m\ell}^2}}{\text{erfc}(\sqrt{\beta_3}\eta_{m\ell})} = \sqrt{\pi}\phi G\eta_{m\ell}\chi_{m\ell} \tag{24}$$

where

$$R_{k2} = \frac{k_2}{k_1}, \qquad R_{k3} = \frac{k_3}{k_1}$$

$$G = \frac{L}{C_{p1}(T_0 - T_{\text{eut}})}, \qquad \beta_2 = \frac{C_{p2} + L\phi(\partial\chi/\partial T_2)}{C_{p1}(k_2/k_1)}$$

$$\beta_3 = \frac{C_{p3}}{C_{p1}}\frac{k_1}{k_3}, \qquad \Theta_1 = \frac{T_{\text{eut}} - T_T}{T_0 - T_{\text{eut}}}$$

$$\Theta_2 = \frac{T_{\text{eut}} - T_{\text{eq}}}{T_0 - T_{\text{eut}}}, \qquad \Theta_3 = \frac{T_{\text{eq}} - T_i}{T_0 - T_{\text{eut}}} \tag{25}$$

Before closing this section, it is worth stressing the purpose of presenting a one-dimensional model, when it is clear from the experimental findings and even from intuition that buoyancy-driven flow in the liquid phase will initiate two-dimensional effects. We believe that it is very constructive and useful to define the region of validity of a simple, easy-to-use model, able to provide engineering estimates for complicated processes exemplified by the present problem. This is achieved by comparing our accurate experimental findings to the predictions of the model for the case of an insulated bottom wall in the next section. If a more accurate model is desired, one has to account for flow in the liquid phase and the mush zone. Note that no unique constitutive equations for flow, heat, and mass transfer in a mushy zone are widely accepted, even though the equations proposed by Bennon and Incropera[6] appear to be promising. Two-dimensional simulations using the Bennon and Incropera[6] equations together with the finite-difference discretization method require the use of supercomputers.[7] This makes the development of simple models, like the present, for engineering estimates well worthwhile.

Table 1 Values of properties used in the theoretical model

c	5%	10%	15%
k_s(W/mK)	2.5	2.5	2.5
k_l(W/mK)	0.582	0.566	0.55
k_b(W/mK)	1.09	1.09	1.09
C_{ps}(J/kgK)	1565	1565	1565
C_{pl}(J/kgK)	4186.8	4184.6	4182.5
C_{pb}(J/kgK)	900	900	900
ϕ	0.35	0.35	0.35
χ	0.375	0.25	0.1
G	25	25	25
T_{eq} (°C)	−3.189	−6.894	−11.063
$\partial\chi/\partial T$	−31.6	−18.565	−15.958

IV. Results and Discussion

The main experimental results document the effects of the initial concentration of the alloy and of the bottom wall heating on the growth of the solid and mixed-phase regions inside

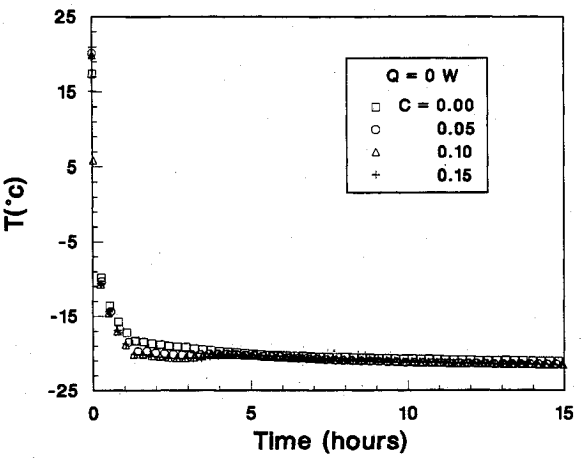

Fig. 3a Top wall temperature variation with time for $Q = 0$ W.

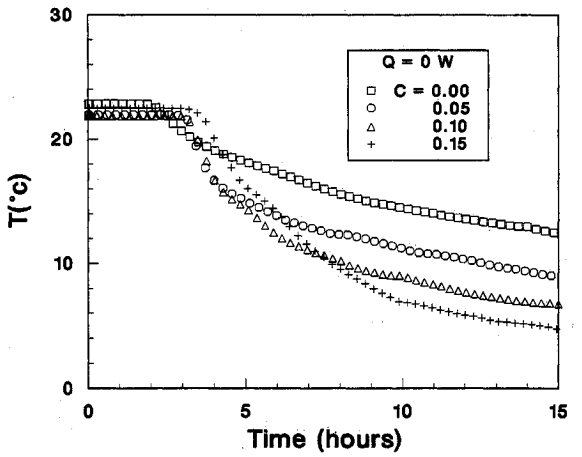

Fig. 3b Bottom wall temperature variation with time for $Q = 0$ W.

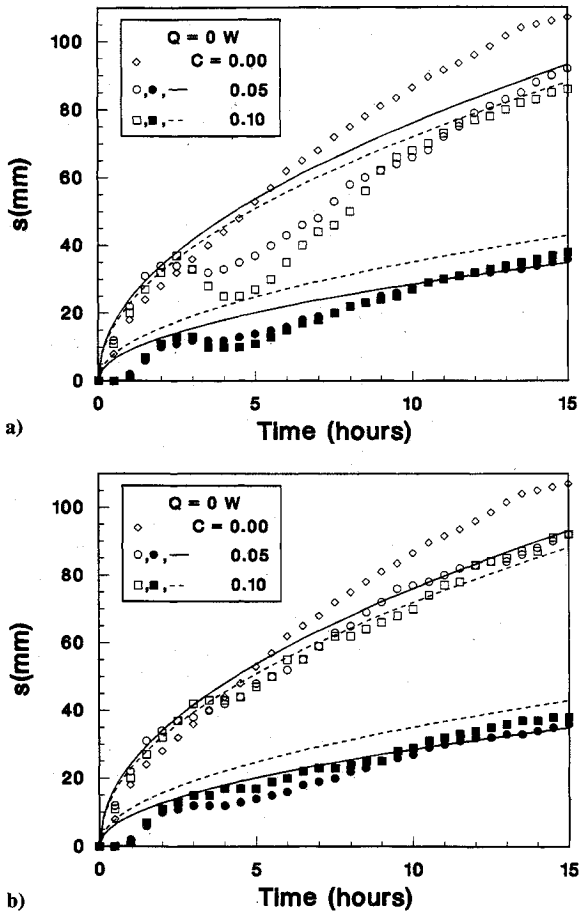

Fig. 4 The growth of the solid/mush (dark symbols) and mush/liquid (open symbols) interfaces for $Q = 0$. The solid lines correspond to the theoretical predictions; a) centerline location, b) 10 cm to the right of the centerline.

the bed of beads. To aid the discussion of the results, the equilibrium phase diagram of the water-ammonium chloride mixture shown in Fig. 2 is presented. According to this diagram, when a liquid mixture of concentration less than about 19 wt % is cooled at static conditions below the temperature of the liquidus curve, ice grows from the liquid mixture creating a mixed-phase region (ice + liquid mixture). The last liquid to solidify forms a eutectic solid mixture of ice and ammonium chloride. On the other hand, if the temperature of a mixture of concentration greater than approximately $C = 0.19$ is lowered below the liquidus temperature, ammonium chloride grows from the liquid.

In the first series of experiments, the top wall of the cavity was cooled by the heat exchanger described earlier. Before it was circulated through the top wall heat exchanger, the coolant temperature was lowered to $-25°C$ in the refrigerator circulator. The temperature of the coolant in the refrigerator circulator remained practically unchanged for the duration of the experiments. Figure 3 shows the dependence of the top (Fig. 3a) and bottom (Fig. 3b) wall temperature on time for different initial alloy concentrations in the cavity. In all cases, the temperature of the top wall decreases rapidly until a plateau is reached. The initial concentration effect on the top wall temperature is practically negligible. The temperature response of the bottom wall is quite different. Because of the large thermal inertia of the saturated porous bed as well as because of the large resistance the presence of the porous bed offers to the buoyancy-driven flow, it takes some time until the cooling effect of the top wall is felt by the bottom wall. After this time, the temperature of the bottom wall decreases monotonically until a plateau is reached. The effect of the initial concentration of the alloy on the bottom wall temperature is significant. As the initial concentration increases, the bottom wall temperature at large times decreases. This result indicates that the liquid mixture needs to be brought down to considerably lower temperatures for the solidification to take place as the concentration increases.

The growth of the mixed-phase region at the centerline of the system and at 50 mm away from the centerline is reported in Figs. 4a and 4b. The symbols correspond to experimental results and the lines to the predictions of the theoretical model. The dark symbols denote the solid/mush interface and the open symbols the mush/liquid interface. At large times, both the interfaces mentioned earlier grow monotonically. What is interesting, however, is the fact that remelting is observed at the mush/liquid as well as the solid/mush interface. The remelting phenomenon is more pronounced at the centerline (Fig. 4a). It appears that the solidification process is underway before the entire fluid body saturating the bed of beads is brought down to a temperature near the solidification temperature. A reason for this fact is the added thermal inertia and resistance to flow offered by the packed bed of beads. As a result, when the "warmer" fluid residing in the bottom wall vicinity is brought into contact with the solidifying region by the action of natural convection, it causes melting and temporary withdrawal of the solid/mush and mush/liquid interfaces. The predictions of the theoretical model appear to be reasonable at large times. However, since the theoretical model does not account for convection, it cannot predict the remelting phenomenon, and it proves to be rather unsuccessful during the time when remelting occurs. The effect of increasing the initial concentration of the alloy is to thicken the solid region and reduce the size of the mushy zone. This fact is more clearly visible in the theoretical results. The experimental results also show the trend but not as clearly because of the presence of the buoyancy-driven flow and the related remelting phenomenon. No mushy zone exists in the limit of pure water solidification ($C = 0$), where the solid and the liquid regions are separated by a sharp interface.

Characteristic temperature profiles at the centerline for $C = 0.15$ are reported in Fig. 5a. The position of the mush/liquid interface is marked by small horizontal lines. It can be observed that the temperature distribution in the liquid region transforms from conduction-type at early times to the convection-type at later times, featuring a practically isothermal core and two thermal layers surrounding it. The temperature distribution in the solid and the mixed-phase regions is linear. With reference to the latter, it appears that the convective motion in the permeable mixed-phase region is not strong enough to alter the linearity of the temperature profile. The theoretical model predicts the temperature distribution rather well at $t = 3$ h when the temperature field is conduction dominated. As time progresses and the buoyancy-driven flow is set in the system, the predictions of the conduction theoretical model become inaccurate, particularly so in the liquid region.

To explore further the effect of the buoyancy-driven flow on the solidification phenomenon, we conducted a series of experiments in which the bottom wall was heated with a constant heat flux by the heater discussed in the previous section. More specifically, at $t = 0$ the coolant was circulated through the top wall heat exchanger, and simultaneously a constant heating rate $Q = 36$ W equally distributed was applied to the bottom wall. This heating condition induced larger temperature gradients in the cavity and enhanced the buoyancy-driven flow.

Figure 6 shows the temperature history of the top and bottom walls at characteristic initial concentrations. The temperature distribution of the top wall appears similar to what was discussed in connection with Fig. 3a; that is, the top wall temperature decreases with time until a plateau is reached and the effect of initial concentration is negligible. On the other hand, the temperature of the bottom wall (Fig. 6b) exhibits features significantly different from what was discussed in Fig. 3b. The constant heat flux applied to the bottom wall increases its temperature initially until a maximum is reached, indicating that the cooling effect of the top wall starts being felt by the

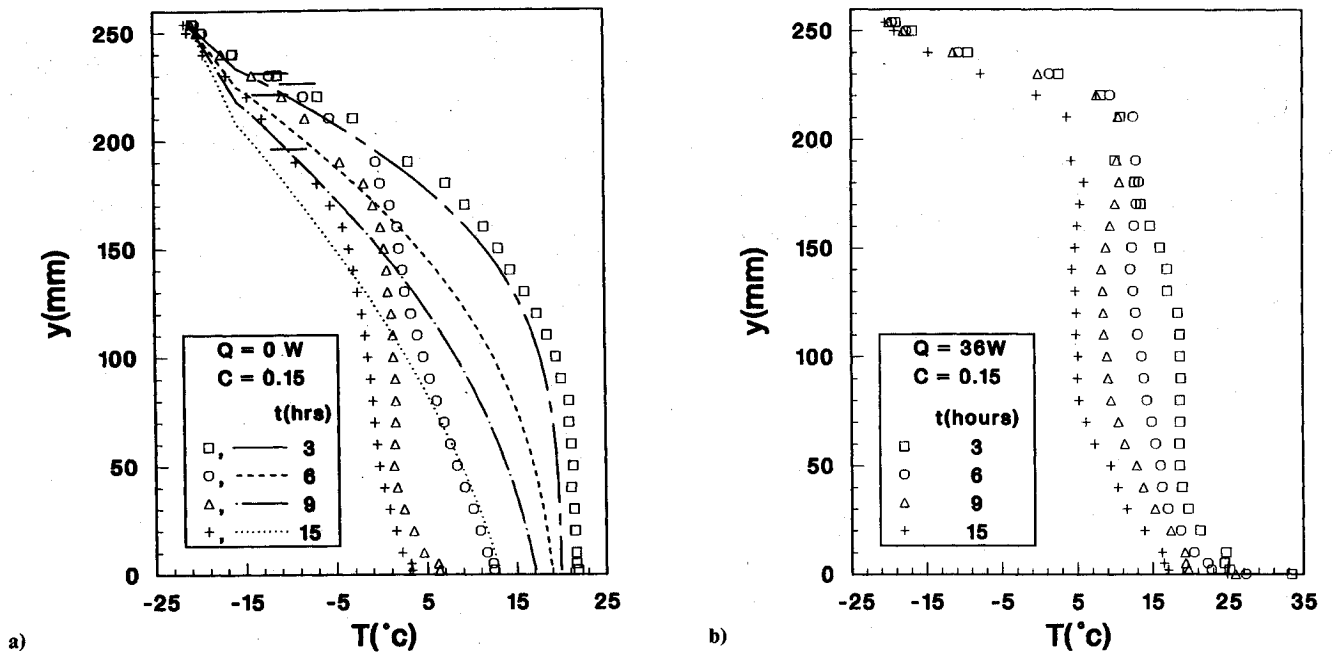

Fig. 5 Temperature variation in the vertical direction at the centerline of the cavity; a) $Q = 0$ W, b) $Q = 36$ W.

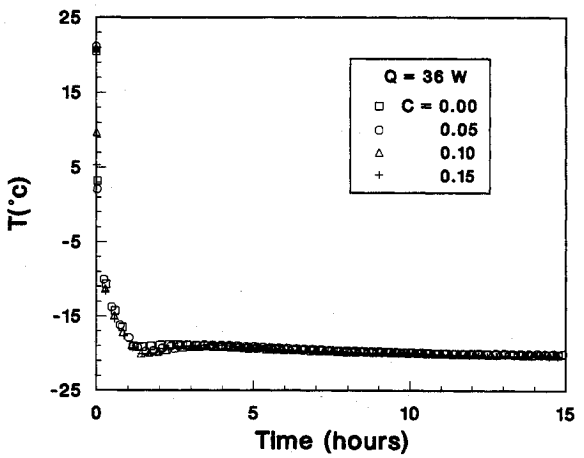

Fig. 6a Top wall temperature variation with time for $Q = 36$ W.

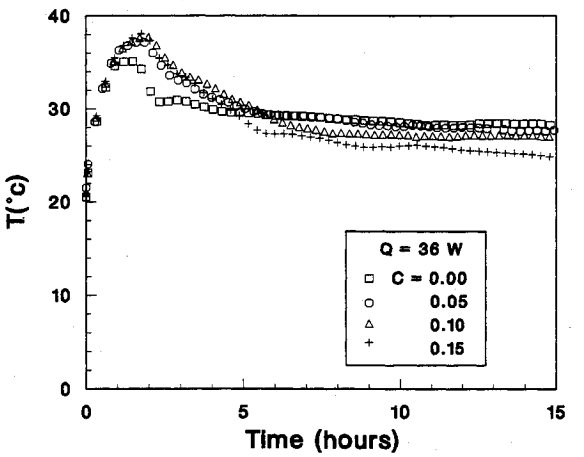

Fig. 6b Bottom wall temperature variation with time for $Q = 36$ W.

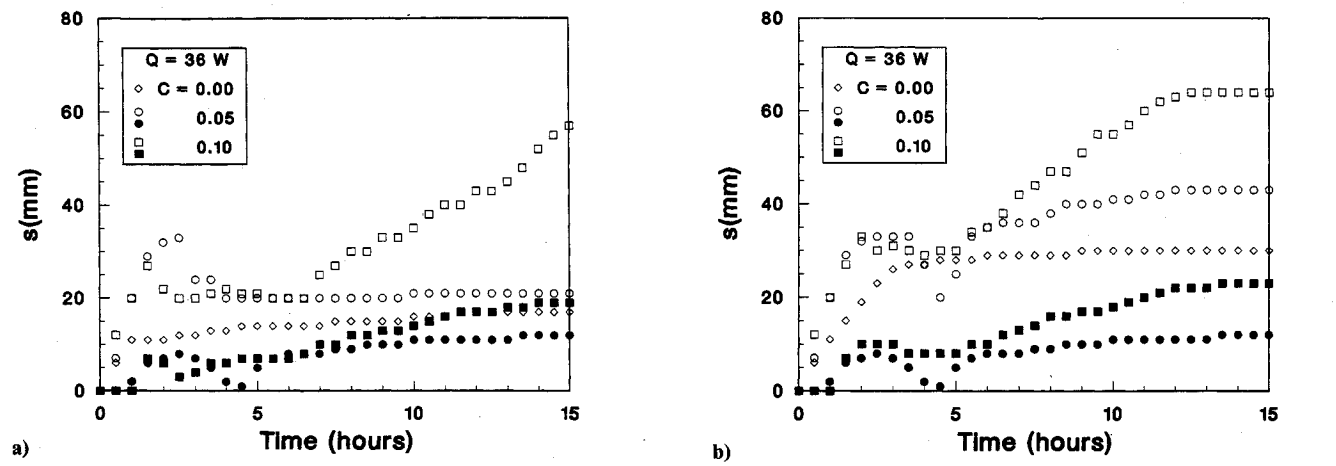

Fig. 7 The growth of the solid/mush (dark symbols) and the mush/liquid (open symbols) interfaces for $Q = 36$ W; a) centerline location, b) 10 cm to the right of the centerline.

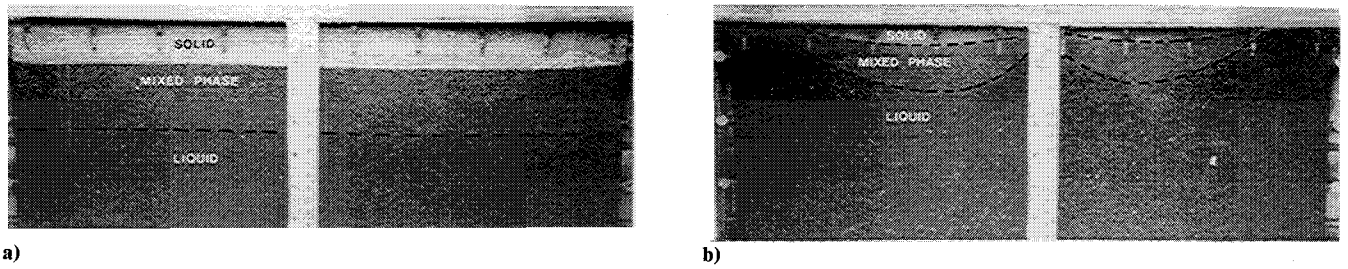

a) b)

Fig. 8 Sequence of photographs illustrating the effect of bottom wall heating on the solidification process; a) $Q = 0$ W, $C = 5\%$, $t = 15$ h; b) $Q = 36$ W, $C = 5\%$, $t = 12$ h.

bottom wall. Thereafter, the temperature decreases until a plateau is reached. Much like in Fig. 3b, increasing the initial concentration decreases the bottom wall temperature. However, this effect is weaker when the bottom wall is heated, as comparison of Figs. 3b and 6b indicates.

The growth of the solid/mush and mush/liquid interfaces is reported in Fig. 7a for the centerline of the system and in Fig. 7b for a location 50 mm to the right of the centerline. In both locations significant remelting takes place. The remelting is considerably more drastic than that which was discussed in connection with Fig. 4 because the results in Fig. 7 are for bottom wall heating $Q = 36$ W. This heating enhances natural convection and increases the temperature of the fluid that comes into contact with the solidifying fronts.

A qualitative comparison of the solid and mushy regions with and without bottom wall heating is presented in the photographs of Fig. 8. Because of the presence of the bed of spheres, it is difficult to photograph clearly the solidifying interfaces. To aid the reader visually, the solid/mush and the mush/liquid interfaces have been traced with dashed lines. The difference between Figs. 8a and 8b is indeed striking. The bottom wall heating strengthens the buoyancy-driven flow and transforms the flat interfaces of Fig. 8a to the severely curved interfaces of Fig. 8b. The shape of the interfaces in Fig. 8b implies that the flowfield consists of four cells. This fact is made clear if one realizes that in the liquid phase directly below the region of maximum thickness of the mushy zone in the left half of Fig. 8b, a liquid "stream" exists moving downward. This stream separates two counterrotating cells filling the left half of the cavity. A similar argument holds for the right half of the cavity. Both the solid and the mixed-phase regions in Fig. 8b are of significantly less extent than those of Fig. 8a.

Finally, the centerline temperature distribution of Fig. 5b indicates the presence of convection in the system at early times. A sharp thermal boundary layer lines the bottom wall throughout the experiment. Once convection sets in the system, the fluid in the core region is visibly warmer when the bottom wall is heated (Fig. 5b) than when it is not (Fig. 5a).

V. Conclusions

In this paper, an experimental study was presented for the problem of freezing of a water-NH_4Cl mixture saturating a packed bed of beads cooled through its top wall. It was found that the solidification takes place in the form of three distinct regions. In the first region, a frozen solid occupies the pores of the packed bed. In the second region, a composite of solid and liquid (mushy zone) occupies these pores. In the third region, the bed is saturated by liquid. These regions are significantly affected in shape and are reduced in size by the presence of constant heat flux heating at the bottom wall. Interestingly, remelting was observed at the solid/mush and the mush/liquid interfaces. This remelting occurs because of the thermal inertia and the flow resistance of the packed bed ("warm" water located away from the solidifying regions reaches these regions well after solidification has started and causes remelting). The remelting phenomenon was more severe when the bottom wall was heated.

The temperature distribution in the solid and the mushy zone was linear, indicating that heat transfer occurs by conduction. Conduction appeared to be the main heat transfer mechanism in the liquid at early times as well, when the bottom wall was insulated. As time progressed, convection took over in the liquid as the major heat transfer mode.

A simplified theoretical mode that neglected the presence of convection naturally did not fair well in predicting the remelting and its impact on the solidification process. In addition, it failed to predict accurately the temperature distribution in the liquid phase when convection was dominant. On the other hand, the theoretical model predicted reasonably well the temperature distribution in the solid and mixed-phase regions as well as in the liquid region before convection became dominant. The theoretical prediction of the growth of the solid/mush and mush/liquid interfaces away from the time of remelting was also acceptable, considering the simplicity of the model. Overall, it is felt that the model may be used when rough estimates of the solidification phenomenon are desired.

Acknowledgment

Support for this work provided by the National Science Foundation through Grant ENG 8451144 is greatly appreciated.

References

[1]O'Callaghan, M. G., Gravalho, E. G., and Huggins, C. E., "An Analysis of Heat and Solute Transport During Solidification of an Aqueous Binary Solution," *International Journal of Heat and Mass Transfer,* Vol. 2, No. 4, 1982, pp. 553–573.

[2]Fang, L. J., Cheung, F. B., Linehan, J. H., and Pederson, D. R., "Selective Freezing of a Dilute Salt Solution on a Cold Ice Surface," *Journal of Heat Transfer,* Vol. 106, No. 6, 1984, pp. 385–393.

[3]Worster, M. G., "Solidification of an Alloy from a Cooled Boundary," *Journal of Fluid Mechanics,* Vol. 167, 1986, pp. 481–501.

[4]Poulikakos, D., "On the Growth of a Solid from a Line Heat Sink in a Binary Alloy," *Numerical Heat Transfer,* Vol. 14, No. 1, 1988, pp. 113–126.

[5]Poulikakos, D., and Cao, W. Z., "Solidification of a Binary Alloy from a Cold Wire or Pipe: Modelling of the Mixed Phase Region," *Numerical Heat Transfer,* Vol. 15, No. 1, 1989, pp. 197–219.

[6]Bennon, W. D., and Incropera, F. P., "A Continuum Model for Momentum, Heat and Species Transport in Binary Solid-Liquid Phase Change Systems-I: Model Formulation," *International Journal of Heat and Mass Transfer,* Vol. 30, No. 10, 1987, pp. 2165–2170.

[7]Bennon, W. D., and Incropera, F. P., "A Continuum Model for Momentum, Heat and Species Transport in Binary Solid-Liquid Phase Change Systems-II: Application to Solidification in a Rectangular Cavity," *International Journal of Heat and Mass Transfer,* Vol. 30, No. 10, 1987, pp. 2171–2187.

[8]Hayashi, Y., and Komori, T., "Investigation of Freezing of a Salt Solution in Cells," *Journal of Heat Transfer,* Vol. 101, No. 3, 1979, pp. 459–464.

[9]Fujii, T., Pourier, D. R., and Flemings, M. C., "Monosegregation in Multicomponent Low Alloy Steel," *Metallurgical Transactions,* Vol. 10B, 1979, pp. 313–319.

[10]Ridder, S. D., Reyes, F. C., Chakravotry, S., Mehrabian, R., Nauman, J. D., Chen, J. H., and Klein, H. J., "Steady State Segregation and Heat Flow in ESR," *Metallurgical Transactions,* Vol. 9R, 1978, pp. 415–425.

[11]Hills, R. N., Loper, D. E., and Roberts, P. H., "A Thermodynamically Consistent Model for a Mushy Zone," *Quaterly Journal of Mechanics and Applied Mathematics,* Vol. 36, No. 4, 1983, pp. 505–539.

[12]Gupta, J. P., and Churchill, S. W., "Heat and Moisture Transfer

in Sand During Freezing," Environmental Geophysical Heat Transfer," WAM of ASME, Washington, DC, Nov. 30, 1971, HTD-Vol. 4.

[13]Frivik, P. E., and Comini, G., "Seepage and Heat Flow in Soil Freezing," *Journal of Heat Transfer,* Vol. 104, No. 2, 1982, pp. 323–328.

[14]Goldstein, M. E., and Reid, R. L., "Effect of Fluid on Freezing and Thawing of Saturated Porous Media," *Proceedings of Royal Society of London,* Series A, Vol. 364, 1978, pp. 45–73.

[15]Sugawara, M., Imaba, H., Seki, N., "Effect on Maximum Density of Water on Freezing of a Water-Saturated Horizontal Porous Layer," *Journal of Heat Transfer,* Vol. 110, No. 1, 1988, pp. 155–159.

[16]Weaver, J. A., and Viskanta, R., "Freezing of Liquid-Saturated Porous Media," *Journal of Heat Transfer,* Vol. 108, No. 3, 1986, pp. 654–659.

[17]Weaver, J. A., and Viskanta, R., "Freezing of Water Saturated Porous Media in a Rectangular Cavity, *International Communications in Heat Mass Transfer,* Vol. 13, No. 3, 1986, pp. 245–252.

[18]Stephen, H., and Stephen, T., *Solubilities of Inorganic and Organic Compounds,* Vol. 1, Pergamon Press, New York, 1963, pp. 212–213.

[19]Dean, J. A. (ed.), *Lange's Handbook of Chemistry,* 12th ed., McGraw-Hill, New York, 1979.

[20]Washburn, E. W. (ed.), *International Critical Tables,* McGraw-Hill, New York, 1929.

[21]Özişik, M. N., *Heat Conduction,* Wiley, New York, 1980.